nutrients

MDPI

Article

Basal Chromatin Accessibility and Heterogeneous Molecular Responses Following Vitamin D_3 Supplementation in Human PBMCs

Maciej Rybiński [1], Emilia Gospodarska [1], Ranjini Ghosh Dastidar [1], Moray J. Campbell [2] and Carsten Carlberg [1,*]

[1] InLife Institute of Animal Reproduction and Food Research, Polish Academy of Sciences, ul. Trylińskiego 18, 10-683 Olsztyn, Poland; m.rybinski@pan.olsztyn.pl (M.R.); e.gospodarska@pan.olsztyn.pl (E.G.); r.dastidar@pan.olsztyn.pl (R.G.D.)

[2] Department of Oncology, Karmanos Cancer Institute, School of Medicine, Wayne State University, Detroit, MI 48201, USA; campbellm@karmanos.org

* Correspondence: c.carlberg@pan.olsztyn.pl; Tel.: +48-604-336-461

Abstract

Background/Objectives: Individuals differ in their molecular response to vitamin D_3 supplementation. We investigated variation in acute chromatin accessibility changes in peripheral blood mononuclear cells (PBMCs), which predominantly comprise lymphocytes and monocytes, and their relationship with gene expression and baseline accessibility. **Methods**: Paired ATAC-seq and RNA-seq profiles were analyzed in 38 healthy VitDPAS participants before (Day 0) and 24 h after (Day 1) a body-weight-adjusted vitamin D_3 bolus of 1000 IU/kg. Exploratory *k-means* clustering used region-level Day 1–Day 0 differences in normalized ATAC-seq signal across 23,244 consensus regions, standardized separately for each region across participants. Chromatin-state annotations, transcription factor motifs and previously mapped vitamin D receptor (VDR)-binding sites were examined. **Results**: Clustering identified accessibility-increase (n = 13), mixed (n = 18) and accessibility-decrease (n = 7) groups. Within-group analyses identified two, zero and three differentially accessible regions, respectively, at false discovery rate (FDR) < 0.05. Nominal significance and signal-abundance filtering yielded 620 candidate regions. RNA-seq identified 74, eight and zero differentially expressed genes in the respective groups at FDR < 0.05, with immune-related pathway enrichment in the accessibility-increase group. Accessibility gains frequently coincided with reduced expression at selected RNA-seq-significant loci. Lower baseline accessibility was associated with subsequent increases, although mathematical coupling, regression to the mean and library signal-to-background variation limit interpretation. **Conclusions**: Normalized PBMC chromatin accessibility changes following vitamin D_3 supplementation varied among participants. The association between baseline accessibility and subsequent change remains descriptive and does not establish predictive value. Controlled, longitudinal and cell-type-resolved studies are needed to distinguish biological responses from compositional and technical variation.

Keywords: vitamin D; chromatin accessibility; ATAC-seq; transcriptome; peripheral blood mononuclear cells; interindividual variability

Check for updates

Academic Editor: Marilyn Cornelis

Received: 15 October 2026
Revised: 11 November 2026
Accepted: 12 November 2026
Published: 13 November 2026

Copyright: © 2026 by the authors. Licensee MDPI, Basel, Switzerland. This article is an open access article distributed under the terms and conditions of the Creative Commons Attribution (CC BY) license.

1. Introduction

Vitamin D_3 modulates innate and adaptive immune functions by altering gene expression in immune cells [1–4]. Most of these genomic effects are mediated by 1α,25-

dihydroxyvitamin D_3 ($1,25(OH)_2D_3$), the biologically active vitamin D metabolite and ligand of the transcription factor vitamin D receptor (VDR) [5]. Ligand-activated VDR binds regulatory regions of the genome, such as enhancers and transcription start site (TSS) regions, and thereby directly or indirectly influences the transcription of vitamin D target genes. However, molecular responses to vitamin D vary among individuals, as demonstrated in PBMCs and donor-derived colonic organoids [6,7].

Vitamin D signaling also depends on the availability and local metabolism of its ligand. Following supplementation, vitamin D_3 is converted to 25-hydroxyvitamin D_3 ($25(OH)D_3$) predominantly in the liver [8]. The enzyme CYP27B1 generates the active metabolite $1,25(OH)_2D_3$ in the kidney and in selected extrarenal cells, including activated immune cells, whereas CYP24A1 contributes to metabolite degradation [8,9]. Consequently, individual responses may depend on precursor availability, local activation and catabolism, VDR abundance, and the identity and activation state of the responding cells [10]. Circulating $25(OH)D_3$ provides information about systemic vitamin D status but does not directly quantify intracellular $1,25(OH)_2D_3$ action.

VDR binding is determined not only by the presence of suitable DNA motifs but also by the underlying chromatin environment. Genome-wide VDR occupancy is strongly context-dependent and frequently occurs at accessible promoters and enhancers together with lineage-determining and signal-responsive transcription factors [11–13]. Chromatin accessibility may therefore determine which regulatory regions can respond to VDR activation and which genes become part of the vitamin D response. ATAC-seq provides a genome-wide measure of accessible chromatin, while its integration with RNA-seq allows changes in regulatory activity to be related to their potential transcriptional consequences [14,15].

PBMC-based supplementation studies have demonstrated interindividual variation in molecular responses to vitamin D_3 [6,16]. Interindividual variability is not restricted to peripheral blood. Paired ATAC-seq and RNA-seq analyses of colonic organoids from genetically diverse donors also revealed donor- and ancestry-associated differences in responses to $1,25(OH)_2D_3$, some of which were linked to *cis*-regulatory genetic variants [7]. Interindividual variation in vitamin D responsiveness has been conceptualized through the personal vitamin D response index [17]. PBMCs provide a readily accessible source of immune cells, and ex vivo studies have demonstrated donor-specific transcriptional responses to $1,25(OH)_2D_3$ [18]. Nevertheless, the epigenomic basis of the variable response remains insufficiently understood. It is unclear whether individuals differ primarily in the magnitude of a shared chromatin response or display distinct, potentially opposing patterns of chromatin remodeling.

Previous work demonstrated interindividual variation in PBMC gene-expression responses to vitamin D_3 supplementation [16]. However, averaging signals across participants can obscure opposing individual responses. Moreover, it has not been determined whether the chromatin state before supplementation is associated with the direction and magnitude of the subsequent response.

We hypothesized that interindividual variability in the response to vitamin D_3 involves differences not only in the magnitude but also in the direction of chromatin accessibility changes and that these differences are associated with the pre-existing chromatin state. To investigate this hypothesis, we analyzed paired ATAC-seq and RNA-seq profiles from PBMCs of 38 healthy adult Caucasian VitDPAS participants, comprising 18 women and 20 men aged 23–64 years, before (Day 0) and 24 h after (Day 1) a body-weight-adjusted vitamin D_3 bolus. We characterized participant-level accessibility patterns, their regulatory annotations and transcription factor motif enrichment, and their relationships with transcriptional changes and reference VDR-binding sites.

2. Materials and Methods

2.1. Study Design, Participants and Vitamin D_3 Intervention

VitDPAS is a single-arm, non-randomized intervention study registered at ClinicalTrials.gov under NCT06104111. Participants received an oral vitamin D_3 bolus of 1000 IU/kg body weight [16]. The present analysis concerns samples obtained immediately before and 24 h after the first bolus. Of the 45 recruited participants, 38 had paired ATAC-seq and RNA-seq datasets meeting the requirements for inclusion in this analysis. The remaining seven participants were excluded because the fraction of reads in peaks (FRiP) of their ATAC-seq data at one or both time points was below 0.1.

Participants were recruited as healthy volunteers according to the eligibility criteria described previously [16]. These included an age of 20–65 years and a body mass index (BMI) of 18.5–29.9 kg/m^2. Relevant exclusion criteria included recent illness or infection, chronic kidney or liver disease, and medications affecting vitamin D or calcium metabolism. All participants were Caucasian. Blood counts, including leukocyte differentials, were not analyzed. Serum 25(OH)D_3 concentrations were measured at baseline (Day 0) and 24 h after supplementation (Day 1). Circulating 1,25$(OH)_2D_3$ concentrations were not measured.

The study protocol was approved by the Ethics Committee of the Olsztyn Chamber of Physicians (approval no. 31/2023/VIII). All participants provided written informed consent before participation. No time-matched untreated control group was included.

2.2. Blood Collection and PBMC Isolation

Blood (8 mL) was collected immediately before, and at 24 h following the oral vitamin D_3 bolus. Within one hour of blood collection, PBMCs were isolated using Vacutainer CPT Cell Preparation Tubes with sodium citrate (Becton Dickinson, Franklin Lakes, NJ, USA). This procedure isolates the mononuclear-cell fraction, composed predominantly of T cells, B cells, NK cells and monocytes. Most granulocytes are excluded by density separation. The analyzed material therefore represents isolated PBMCs rather than an unfractionated leukocyte preparation. Direct immunophenotyping of the isolated PBMCs was not performed. Cell composition was estimated computationally from the bulk RNA-seq profiles, as described in Section 2.7. Isolated cells were washed with phosphate-buffered saline, aliquoted at a concentration of 4×10^6 cells/mL, and stored at –80 °C for subsequent chromatin accessibility and transcriptomic analyses.

2.3. ATAC-seq and RNA-seq Library Preparation and Sequencing

For ATAC-seq, nuclei were isolated from 100,000 PBMCs by incubation in 50 µL lysis buffer (10 mM Tris-HCl, pH 8.0; 10 mM NaCl; 3 mM $MgCl_2$; 0.1% Tween-20; 0.1% IGEPAL CA-630; 0.01% digitonin). After 3 min on ice, 1 mL of wash buffer (10 mM Tris-HCl, pH 8.0; 10 mM NaCl; 3 mM $MgCl_2$; 0.1% Tween-20) was added. Nuclei were pelleted and subjected to transposition using a Tn5 transposase reaction mix (Illumina, Inc., San Diego, CA, USA), supplemented with 0.01% digitonin and 0.1% Tween-20. The transposition reaction was carried out at 37 °C for 30 min in a thermomixer. Transposed DNA was purified using the DNA Clean & Concentrator-5 Kit (Zymo Research, Irvine, CA, USA), followed by PCR amplification, purification, and size selection with SPRIselect beads (Beckman Coulter, Inc., Brea, CA, USA). Library quality was assessed using an Agilent TapeStation (Santa Clara, CA, USA). Indexed libraries were quantified, pooled, and prepared for sequencing. For RNA-seq, total RNA was extracted from PBMCs using the High Pure RNA Isolation Kit (Roche, Penzberg, Germany), following the manufacturer's instructions. RNA quality was evaluated on an Agilent TapeStation. Ribosomal RNA was depleted using kits from New England Biolabs (Ipswich, MA, USA), and libraries were prepared according to the manufacturer's protocols. ATAC-seq and RNA-seq libraries were sequenced with 75 bp

paired-end and single-end reads, respectively, on a NextSeq 2000 platform (Illumina) at the EMBL GeneCore Facility (Heidelberg, Germany), following standard protocols. Adapter sequences were removed from ATAC-seq reads using TrimGalore (v0.6.10), which uses cutadapt (v4.6) for adapter trimming and quality filtering prior to alignment.

2.4. ATAC-seq Preprocessing, Quality Control and Differential Chromatin Accessibility Analysis

ATAC-seq reads were aligned to GRCh38.p14 using the STAR aligner (v2.7.10b) in paired-end mode, with no 5′ or 3′ read clipping (–clip5pNbases 0 –clip3pNbases 0), –seedSearchStartLmax 50, –alignEndsType Local, –alignEndsProtrude 0 ConcordantPair, and –outFilterMismatchNmax 10; output BAM files were sorted by coordinate (–outSAMtype BAM SortedByCoordinate) with all SAM attributes retained (–outSAMattributes All). Alignments were filtered to remove reads mapping to alternative/non-primary contigs and to the mitochondrial genome. Peaks were called from deduplicated paired-end alignments using MACS3 (v3.0.0b1) in BAMPE mode, with an effective human genome size specified by -g hs and a q-value threshold of 0.01. MACS3 used the observed paired-end fragment lengths. Peaks overlapping the ENCODE blacklisted regions for GRCh38 (hg38-blacklist.v2.bed) were excluded. Unique-read counts denote the numbers of non-duplicate read alignments with MAPQ $\geq$ 30 retained in the final BAM files after removal of mitochondrial and alternative-contig alignments. TSS enrichment scores were calculated from these BAM files using the TSSEscore() function in ATACseqQC (v1.36.1), with default parameters and TSSs defined using TxDb.Hsapiens.UCSC.hg38.knownGene. The score summarizes the maximum aggregate enrichment around TSSs relative to flanking background (Table S1). Differential chromatin accessibility analysis was conducted in R (v4.4.0) on macOS 12.6 using the DiffBind package (v3.8.4). A consensus peak set was generated using the dba.count function with summits set to 75, followed by merging of overlapping summits, yielding 23,945 peak summits. This set was further filtered to retain only regions detected in more than one sample and to remove regions with more than one zero or missing value, yielding a final consensus set of 23,244 accessible chromatin regions (Table S2). Read counts were normalized using the RLE (relative log expression) method. Peak annotation was performed using the ChIPseeker package (v1.40.0), in combination with the TxDb.Hsapiens.UCSC.hg38.knownGene annotation database (v3.16.0) and the org.Hs.eg.db package (v3.16.0). For each participant and time point, mean accessibility was calculated as the arithmetic mean of normalized read counts across the complete consensus peak set. These participant-level means were used for descriptive visualization and analyses of basal accessibility. Differential accessibility between Day 0 and Day 1 was assessed separately within each responder group using DESeq2 through DiffBind, with participant identity included in the design to account for paired sampling [19].

2.5. Responder Classification

For each participant, Day 1–Day 0 differences in normalized ATAC-seq signal at each of the 23,244 consensus regions were used as input variables for *k-means* clustering. Clustering was performed on the resulting 38 × 23,244 matrix after standardizing each region (z-scores), using the R function kmeans(), with k = 3, random seed 123 and nstart = 1. The clusters were labeled accessibility-increase, mixed and accessibility-decrease according to the direction and magnitude of their mean level Day 1−Day 0 differences. These labels represent an exploratory stratification of continuous variation and were not treated as independently established biological phenotypes.

For the descriptive classification of individual peak-participant pairs, normalized ATAC-seq signals at Day 0 and Day 1 were rounded to the nearest integer. A peak was classified as showing increased, decreased or unchanged accessibility when its rounded

Day 1 value was greater than, smaller than or equal to its rounded Day 0 value, respectively. This peak-level classification was separate from the *k-means* classification of participants and did not indicate statistical significance.

Principal component analysis (PCA) was performed with participants as observations and ATAC-seq regions as variables. For each region and participant, the accessibility change was calculated as $\log_2(\text{SDay1} + 1) - \log_2(\text{SDay0} + 1)$, where S denotes the normalized ATAC-seq signal. Changes were mean-centered and scaled to unit variance across participants for each region before analysis using prcomp() in R. Figure S1B included the complete set of 23,244 consensus regions.

2.6. Transcription Factor Motif Analysis and ChromHMM Annotation

Motif enrichment was analyzed using HOMER v5.1 [20], with the nominal candidate regions from each responder group as the target set and HOMER's default GC-content-matched genomic background as the background. Regions were analyzed using a fixed 200 bp window centered on the peak summit, with no additional background-matching procedure beyond HOMER's default GC correction; the analysis was repeated separately for each responder subgroup, restricted to regions nominally significant at $p < 0.05$. Motifs were evaluated using HOMER's default binomial test, and the default Benjamini-corrected q-value procedure was applied. For ChromHMM annotation, accessible regions were defined separately for each participant and time point using sample-specific MACS3 peak calls at $q < 0.01$. These regions were intersected with the Roadmap Epigenomics E062 reference annotation for primary mononuclear cells from peripheral blood, using the core 15-state ChromHMM model and coordinates lifted over from hg19 to GRCh38 [21,22]. For each sample, the enhancer-associated proportion was calculated as the number of accessible peaks overlapping enhancer-associated states divided by the total number of accessible peaks. This analysis used sample-specific peak sets, and the reference chromatin-state annotations remained fixed across participants and time points.

2.7. RNA-seq Processing and Differential-Expression Analysis

Quality control of RNA-seq data was performed using FastQC (v0.11.9). Single-end, reverse-stranded cDNA reads were aligned to the GRCh38.p14 human reference genome (GENCODE release 43) using the STAR aligner (v2.7.2a). Read quantification was carried out with featureCounts (v2.0.1). Gene annotation, including Ensembl gene identifiers, gene symbols, descriptions, genomic coordinates, biotypes, and Entrez Gene IDs, was retrieved from the Ensembl database (release 100) using the R packages biomaRt (v2.54.1) and org.Hs.eg.db (v3.16.0). Genes lacking HGNC symbols or encoded by the mitochondrial genome were excluded. For downstream analyses, only protein-coding genes were retained. Differential gene expression analysis was conducted in R (v4.4.0) using the DESeq2 package (v1.44.0) [19]. Response direction was assigned from the sign of the DESeq2 $\log_2$FC estimate for Day 1 relative to Day 0. Arithmetic means of raw read counts were provided for descriptive purposes and were not used to classify response direction (Table S3).

Immune-cell composition was estimated from the paired Day 0 and Day 1 bulk PBMC RNA-seq profiles using CIBERSORTx [23]. Samples were assigned to the chromatin accessibility response groups defined by ATAC-seq. Estimated fractions were compared between responder groups at baseline and between paired Day 0 and Day 1 samples within each group.

2.8. Integration of ATAC-seq, RNA-seq and VDR ChIP-seq

Consensus ATAC-seq peaks were linked to genes that were differentially expressed in accessibility-increase responders at FDR < 0.05 using genomic proximity, whereby each

peak was assigned to a gene based on its distance from that gene's TSS, defined according to the strand (the gene's start position for genes on the plus strand, and end position for genes on the minus strand). Peaks within 500 bp of an associated gene's TSS were classified as TSS-proximal. Peaks more than 500 bp and up to 500 kb from that TSS were classified as distal gene-associated regions. Representative peaks were selected independently within the TSS-proximal window (distance ≤ 500 bp from the TSS) and the distal window (distance > 500 bp and ≤500 kb from the TSS). When several TSS-proximal peaks were available for a gene, the peak closest to its TSS was selected. When several distal peaks were available, the peak with the highest ATAC-seq signal was selected. Thus, a gene could be represented by one TSS-proximal peak and one distal peak. Overlap with VDR-binding sites was determined by comparing genomic coordinates using the R package GenomicRanges (v1.50.2). VDR-binding-site coordinates previously determined by ChIP-seq in THP-1 cells [24] served as the reference dataset for VDR-binding sites.

2.9. Functional Enrichment Analysis

Functional enrichment analysis was performed on the 74 genes differentially expressed in accessibility-increase chromatin responders at an FDR threshold of 0.05 (Table S3), using the clusterProfiler (v4.6.2) package in R to query the KEGG (2026) [25], WikiPathways (2024) [26] and Reactome (2024) [27] pathway databases. For each pathway database, the background comprised genes eligible to be identified as differentially expressed in the accessibility-increase analysis, intersected with the genes annotated in that database. Enrichment *p*-values were adjusted using the Benjamini–Hochberg procedure.

2.10. Statistical Analysis

Participants, rather than individual ATAC-seq peaks, were treated as the experimental units in analyses of participant-level summary measures. Differential chromatin accessibility and differential gene expression were analyzed separately within each responder group using paired DESeq2 models that included participant identity and sampling time, thereby accounting for the paired Day 0–Day 1 design. Unless otherwise stated, *p*-values from genome-wide analyses were adjusted for multiple testing using the Benjamini–Hochberg procedure. ATAC-seq regions meeting only the nominal threshold of $p < 0.05$ were considered exploratory candidate regions and were not interpreted as statistically significant after multiple-testing correction. Exploratory candidate regions were required to meet nominal $p < 0.05$ and to have a normalized signal above 10 in every sample of the respective group, as documented in Table S2. These selection criteria were applied separately within each accessibility group and yielded 162, 337 and 143 candidate regions, respectively. At FDR < 0.05, two regions were identified in accessibility-increase responders, none in mixed responders and three in accessibility-decrease responders.

Day 0 and Day 1 proportions of accessible regions assigned to enhancer states were compared separately within each responder group, with participants treated as paired experimental units. Normality of the within-participant Day 1–Day 0 differences was assessed using the Shapiro–Wilk test. Two-sided paired t-tests were used for the mixed and accessibility-decrease responder groups. Because the differences in the accessibility-increase responder group did not meet the normality assumption (Shapiro–Wilk $p = 0.0152$), this group was analyzed using a two-sided Wilcoxon signed-rank test. *p*-values from the three group-wise comparisons were adjusted using the Benjamini–Hochberg procedure. Because the responder groups were defined using Day 0 and Day 1 accessibility data, these comparisons were considered exploratory and did not constitute independent validation of the responder classification. Unique-read counts and TSS scores were compared among the three chromatin responder groups using Kruskal–Wallis tests, separately for Day 0, Day 1

and within-participant $\log_2$(Day 1/Day 0) changes. *p*-values were adjusted across these six ATAC-seq comparisons using the Benjamini–Hochberg procedure. Corresponding analyses of RNA-seq unique-read counts were adjusted across three comparisons. Associations involving accessibility-derived metrics were considered descriptive and did not constitute independent validation of the responder classification.

Responder groups were derived from standardized region-level Day 1–Day 0 differences in normalized accessibility. Participant-level mean signals were subsequently used to summarize and visualize the resulting groups. Because these summaries were calculated from the same paired measurements used for clustering, they were analyzed descriptively and did not provide independent validation of the classification. Paired t-tests and Wilcoxon signed-rank tests were two-sided.

Baseline differences in estimated immune-cell fractions among the three responder groups were assessed using Kruskal–Wallis tests. Within-group Day 0–Day 1 differences were assessed using two-sided Wilcoxon signed-rank tests, matching samples by participant. Benjamini–Hochberg correction was applied separately across the 12 baseline comparisons of estimated cell fractions and across the 36 within-group Day 0–Day 1 comparisons, comprising 12 cell fractions in each of the three responder groups.

2.11. Use of Generative AI-Assisted Technologies

During manuscript preparation, ChatGPT, GPT-6 Astra (OpenAI) was used to assist with language editing and improving clarity and conciseness. All scientific content and suggested revisions were critically reviewed and verified by the authors, who take full responsibility for the final manuscript.

3. Results

3.1. Interindividual Variation in Normalized PBMC Chromatin Accessibility

Paired ATAC-seq profiles from the 38 included participants yielded 23,244 consensus accessible chromatin regions (Table S2). The direction of normalized signal changes varied substantially among participants (Figure S1A). Exploratory *k-means* clustering of standardized region-level Day 1–Day 0 differences in normalized ATAC-seq signal across the 23,244 consensus regions identified accessibility-increase (n = 13), mixed (n = 18) and accessibility-decrease (n = 7) groups (Figure S1B). Demographic characteristics, BMI and serum vitamin D measurements are summarized for the complete analysis population and the exploratory accessibility groups in Table 1.

Table 1. Characteristics of the 38 analyzed participants and their exploratory accessibility groups. Values are mean ± SD. Paired changes were calculated as Day 1–Day 0 for each participant.

Characteristic	All	Accessibility-Increase	Mixed	Accessibility-Decrease
Participants, n	38	13	18	7
Female/male, n	18/20	4/9	11/7	3/4
Age, years	39.1 ± 9.2	40.5 ± 11.4	37.6 ± 9.0	40.1 ± 3.8
Age range, years	23–64	25–64	23–49	37–48
BMI, kg/m^2	23.8 ± 3.1	24.4 ± 3.4	23.4 ± 3.0	23.5 ± 3.3
Serum 25(OH)D_3, Day 0, ng/mL	26.2 ± 10.4	26.0 ± 13.3	26.3 ± 9.0	26.2 ± 9.1
Serum 25(OH)D_3, Day 1, ng/mL	32.6 ± 10.2	31.9 ± 11.9	33.0 ± 9.5	32.9 ± 9.6
Paired change in 25(OH)D_3, ng/mL	6.4 ± 2.6	5.9 ± 2.8	6.7 ± 2.4	6.7 ± 3.0

Participant trajectories and distributions of mean ATAC-seq signals summarize the groups obtained from region-level clustering (Figure S2). Because these summaries use the

same paired measurements as the clustering, they are descriptive and do not independently validate the classification.

Unique-read counts did not differ significantly among the responder groups at Day 0 or Day 1, or in their within-participant FC (all $p_{adj} \geq 0.442$; Table S1). By contrast, the reported TSS scores differed among groups at baseline and after supplementation ($p_{adj} = 0.0167$ and 0.0178, respectively), and their paired fold changes (FC) differed markedly ($p_{adj} = 4.99 \times 10^{-6}$). Median TSS scores increased from 18.36 to 27.24 in accessibility-increase responders, remained comparatively stable in mixed responders, and decreased from 27.39 to 17.94 in accessibility-decrease responders. Median FRiP values increased from 0.14 to 0.22 in accessibility-increase responders, changed from 0.20 to 0.19 in mixed responders, and decreased from 0.26 to 0.16 in accessibility-decrease responders. FRiP, TSS enrichment and accessibility measures were derived from the same libraries, and their covariation does not distinguish biological accessibility changes from variation in library signal-to-background.

Changes in normalized ATAC-seq signals were distributed across the chromosomes (Figure S3). The numbers of regions exceeding the descriptive signal threshold of 100 increased in accessibility-increase responders, changed comparatively little in mixed responders, and decreased in accessibility-decrease responders.

Across the complete consensus set, two, zero and three regions met FDR < 0.05 in the accessibility-increase, mixed and accessibility-decrease groups, respectively (Table 2). Applying the exploratory nominal-significance and signal-abundance criteria yielded 162, 337 and 143 candidate regions, with a union of 620 regions (Figure 1A,B). Of these, 598 met the selection criteria in only one group. This limited overlap does not establish statistically different responses between groups.

Table 2. Summary of molecular findings within the exploratory accessibility groups. Candidate ATAC-seq regions met nominal $p < 0.05$ and the requirement for normalized signal above 10 in every sample of the respective group. Their union comprised 620 regions because the group-specific sets overlapped. Differences in discovery counts do not establish differences in response magnitude between groups.

Outcome	Accessibility Increase	Mixed	Accessibility Decrease
Participants, n	13	18	7
ATAC regions at FDR < 0.05	2	0	3
Exploratory ATAC candidate regions	162	337	143
RNA-seq differentially expressed genes (DEGs) at FDR < 0.05	74	8	0
Upregulated/downregulated DEGs	29/45	0/8	0/0

Mean signals and individual trajectories across the selected candidate regions illustrated the accessibility patterns within each group (Figure 1C,D). PCA of the combined candidate set similarly visualized the structure of the selected data rather than providing independent validation (Figure S4A).

Candidate regions were distributed across the chromosomes and showed enrichment for motifs associated with hematopoietic transcription factors (Figure S4B,C). ETS1, NFY and BCL11B motifs occurred among the enriched motifs in more than one group, whereas ATF1 and KLF5, ELF4 and SP1, and JUN-FOS featured in the accessibility-increase, mixed and accessibility-decrease sets, respectively. These enrichments identify candidate regulatory sequences but do not demonstrate transcription factor occupancy or statistically different motif enrichment between groups.

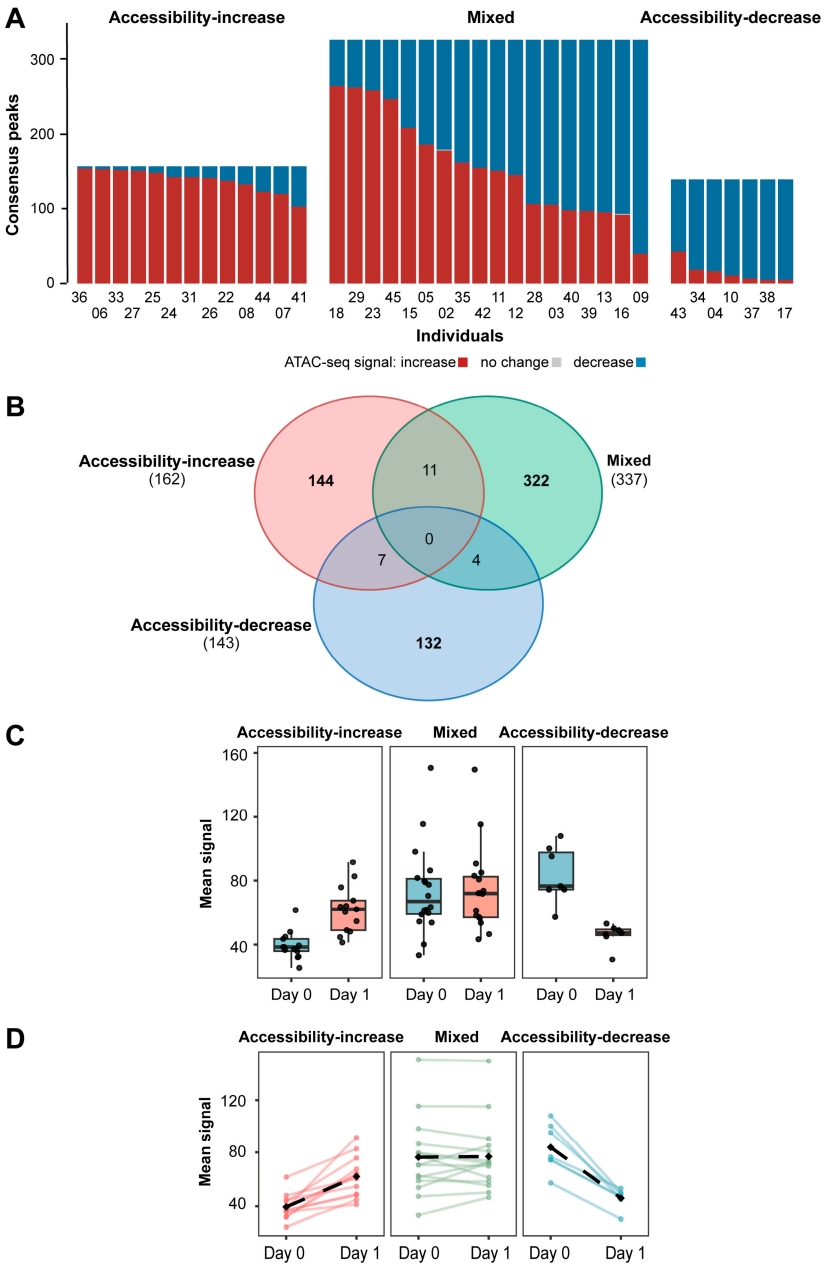


Figure 1. Exploratory characterization of candidate accessibility changes within the three response groups. Distribution of group-specific candidate regions among individual accessibility-increase (n = 13), mixed (n = 18) and accessibility-decrease (n = 7) responders (**A**). Paired Day 0-Day 1 analyses identified 162, 337 and 143 candidate regions at nominal $p < 0.05$ in the accessibility-increase, mixed and accessibility-decrease groups, respectively; this threshold does not establish significance after multiple-testing correction. For each participant, these regions were classified according to increased accessibility at Day 1 (red), decreased accessibility (blue) or equal rounded signal values (gray), using the descriptive classification defined in the Methods section. Venn diagram showing the overlap between the candidate regions identified in the three response groups (**B**). Paired Day 0–Day 1 analyses identified 162, 337 and 143 candidate regions meeting nominal $p < 0.05$ and the requirement for normalized signal above 10 in every sample of the respective group. Box plots showing participant-level mean ATAC-seq signal across the group-specific candidate regions at baseline (Day 0) and 24 h after vitamin D_3 supplementation (Day 1) (**C**). Boxes indicate the median and interquartile range, whiskers indicate 1.5× the interquartile range, and points represent individual participants. Individual changes in mean ATAC-seq signal between Day 0 and Day 1 across the group-specific candidate regions (**D**). Each colored line represents one individual, while dashed black lines connect the group means.

3.2. Transcriptional Responses Within the Chromatin Accessibility Response Groups

Paired RNA-seq analyses identified 74, eight and zero DEGs at FDR < 0.05 in the accessibility-increase, mixed and accessibility-decrease groups, respectively (Table 2 and Table S3). The accessibility-increase group contained 29 upregulated and 45 downregulated genes; all eight DEGs in the mixed group were downregulated. Seven genes, *CXCR4*, *DUSP1*, *KLF11*, *NAMPT*, *PER1*, *TNFAIP3* and *TSC22D3*, were downregulated at FDR < 0.05 in both accessibility-increase and mixed responders. SOCS3 met this threshold only in mixed responders. The remaining 67 DEGs met the threshold only in accessibility-increase responders (Figure 2A). These differences in threshold crossing do not constitute a formal test of differential responsiveness between groups.

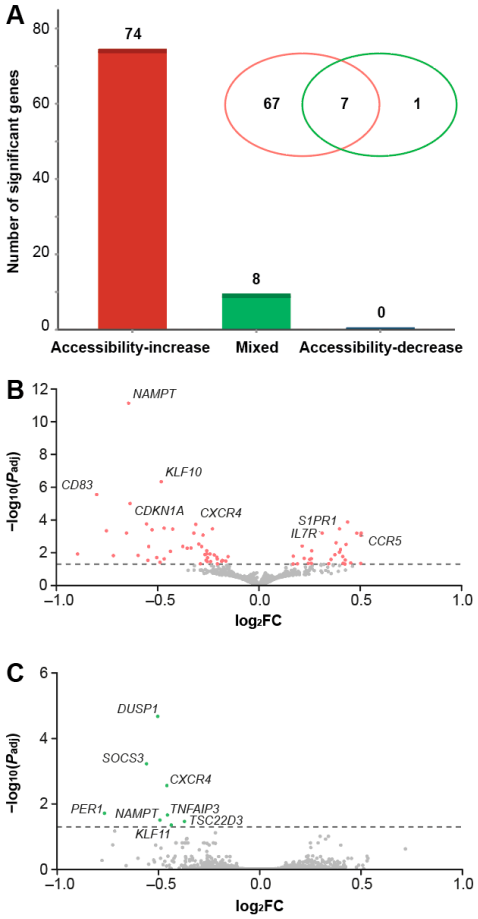


Figure 2. ATAC-seq-based stratification reveals transcriptomic responses within the chromatin accessibility response groups to vitamin D_3 in PBMCs. Number of differentially expressed genes identified by paired comparison of the Day 0 and Day 1 RNA-seq profiles in accessibility-increase (n = 13), mixed (n = 18) and accessibility-decrease (n = 7) responders at an FDR threshold of 0.05 (**A**). The inset Venn diagram shows the overlap between the 74 genes identified in accessibility-increase responders and the eight genes identified in mixed responders. Sixty-seven genes met the FDR threshold only in accessibility-increase responders, one only in mixed responders, and seven in both groups. No differentially expressed gene was identified in accessibility-decrease responders. Volcano plot of the transcriptional response in accessibility-increase responders (**B**) and in mixed responders (**C**). For panels (**B**,**C**), the horizontal axis indicates the $\log_2$FC at Day 1 relative to Day 0, and the vertical axis indicates $-\log_{10}$ of the adjusted *p*-value. Red points in panel B and green points in panel C indicate genes with FDR < 0.05 in accessibility-increase and mixed responders, respectively; gray points indicate genes that did not meet this threshold. The horizontal dashed line marks FDR = 0.05. Selected differentially expressed genes are labeled.

Exploratory analyses at nominal $p < 0.05$ identified 836, 462 and 393 genes in the respective groups (Figure S5). These nominal findings were not interpreted as discoveries surviving multiple-testing correction.

To relate transcriptional responses to local chromatin accessibility, we examined consensus ATAC-seq peaks associated with *NAMPT* and *DUSP1* as representative examples (Figure S6). At the *NAMPT*-associated region, accessibility increased between Day 0 and Day 1 in accessibility-increase responders, changed comparatively little in mixed responders and decreased markedly in accessibility-decrease responders (Figure S6A). *NAMPT* expression was significantly downregulated in both accessibility-increase and mixed responders. At the *DUSP1*-associated region, accessibility increased in accessibility-increase responders, remained comparatively stable in mixed responders and decreased in accessibility-decrease responders (Figure S6B), whereas *DUSP1* expression was significantly reduced in both accessibility-increase and mixed responders. These examples illustrate that accessibility at an assigned gene-associated region was not invariably concordant with the corresponding transcript change.

Functional enrichment analysis of the 74 DEGs identified in accessibility-increase responders highlighted immune signaling pathways (Figure S7). Reactome terms included signaling by interleukins (ILs), IL4 and IL13 signaling, IL7 signaling, chemokine receptor interactions, CD28-family co-stimulation, T-cell receptor signaling and PD-1 signaling. KEGG and WikiPathways analyses similarly identified cytokine–receptor interactions, hematopoietic cell lineage, T-cell receptor signaling and T_H1, T_H2 and T_H17 cell differentiation. Several infection- and cancer-related pathway annotations reflected the inclusion of shared cytokine and lymphocyte signaling genes rather than evidence of infection or malignancy in the participants.

3.3. Chromatin-State Annotation and Integration with Gene-Expression Responses

ChromHMM annotation was used to characterize the regulatory context of accessible regions called separately for each participant and time point. Across all three response groups, most ATAC-seq regions were assigned to TSS-associated chromatin states, while smaller proportions were classified as enhancer-associated or other states (Figure S8A). However, the proportion of accessible regions assigned to enhancer states changed differently between the responder groups. It increased between Day 0 and Day 1 in accessibility-increase responders ($p_{adj} = 0.0068$), showed a smaller and non-significant decrease in mixed responders ($p_{adj} = 0.11$), and decreased markedly in accessibility-decrease responders ($p_{adj} = 0.00267$; Figure S8B). These findings indicate changes in the representation of accessible regions carrying reference enhancer annotations; they do not demonstrate transitions between chromatin states.

To examine the relationship between chromatin accessibility and gene expression, we focused on ATAC-seq peaks assigned to genes that were differentially expressed in accessibility-increase responders at FDR < 0.05. Regions were classified according to their distance from the associated TSS, yielding 58 TSS-proximal and 68 distal peak-gene associations. These 126 peak-gene associations involved 72 unique genes. Of these, three TSS-proximal regions and ten distal gene-associated regions overlapped VDR-binding sites experimentally defined in THP-1 cells [24]. In accessibility-increase responders, nearly all analyzed TSS-proximal regions showed increased chromatin accessibility, whereas expression of most associated genes decreased. Consequently, most TSS peak-gene associations without VDR binding site overlap were in the quadrant representing increased accessibility and reduced gene expression (Figure 3A). The three VDR-overlapping TSS regions showed heterogeneous expression responses: two combined increased accessibility with increased expression, whereas one combined increased accessibility with reduced expression. The

small number of VDR-overlapping TSS regions precluded a meaningful comparison with regions lacking VDR binding site overlap.

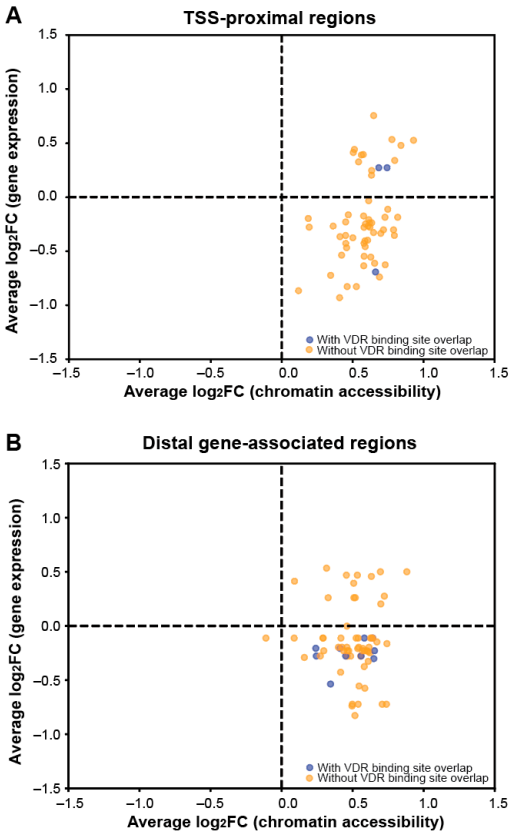


Figure 3. Relationship between chromatin accessibility and gene expression at RNA-seq-significant loci. The analysis was restricted to ATAC-seq peaks assigned to genes that were differentially expressed in accessibility-increase responders at FDR < 0.05. Scatter plots compare the group-averaged ATAC-seq $\log_2$FC with the RNA-seq $\log_2$FC of the associated gene at Day 1 relative to Day 0. TSS-proximal regions comprising 58 peak-gene associations, of which three overlapped an experimentally defined VDR binding site and 55 did not (**A**). Distal gene-associated regions comprising 68 peak-gene associations, of which ten overlapped a VDR binding site and 58 did not (**B**). Each point represents one peak-gene association. The 126 peak-gene associations represent 72 unique genes. VDR-binding-site annotations were obtained from published THP-1 ChIP-seq data [24] and were not measured in the participants' PBMCs. Regions with VDR binding site overlap are shown in blue and those without overlap in orange. Horizontal and vertical dashed lines indicate a $\log_2$FC of zero and divide the plots into quadrants representing the possible combinations of increased or decreased accessibility and gene expression.

A similar pattern was observed at distal gene-associated regions. Most of them displayed increased accessibility in accessibility-increase responders, while expression of the associated genes decreased (Figure 3B). This inverse pattern predominated among regions both with and without VDR binding site overlap. Thus, increased accessibility at the analyzed TSS-proximal and distal gene-associated regions was not generally accompanied by increased transcript abundance of the associated gene.

Comparison across the three responder groups further illustrated the distinct behavior of chromatin accessibility and gene expression (Figure S9). For both TSS-proximal and distal gene-associated regions, ATAC-seq changes shifted from predominantly reduced accessibility in accessibility-decrease responders to increased accessibility in accessibility-increase responders, with mixed responders showing intermediate values. This pattern occurred irrespective of VDR binding site overlap and reflected the ATAC-seq-based defi-

nition of the response groups. By contrast, expression of the associated genes remained predominantly reduced and varied less consistently across the three groups. The clearest inverse relationship was therefore observed in accessibility-increase responders, in whom increased accessibility was frequently accompanied by decreased expression.

Only three TSS-proximal and ten distal gene-associated regions overlapped VDR-binding sites, compared with 55 and 58 regions without VDR overlap, respectively. Any differences between the VDR-overlapping and non-overlapping subsets should therefore be considered descriptive. Moreover, because the analyzed loci were selected according to significant RNA-seq changes in accessibility-increase responders, the distribution of expression changes in this group is selection-dependent and does not provide an independent statistical test of accessibility-expression coupling.

3.4. Basal Chromatin Accessibility Is Inversely Associated with the Acute Response to Vitamin D_3

We next investigated whether basal chromatin accessibility was associated with the magnitude and direction of the acute response to vitamin D_3. Across all 38 participants, the mean ATAC-seq signal at Day 0 showed a pronounced association with the $\log_2$FC between Day 0 and Day 1 (Figure 4). Individuals with comparatively low basal accessibility generally displayed increased accessibility after supplementation and were predominantly classified as accessibility-increase responders. Conversely, individuals with high basal accessibility generally showed decreased accessibility and were enriched among accessibility-decrease responders, while mixed responders occupied an intermediate range. These findings revealed an inverse association between basal accessibility and the subsequent accessibility change. Because the baseline signal also enters the calculation of the response, this association is descriptive and does not independently establish predictive value.

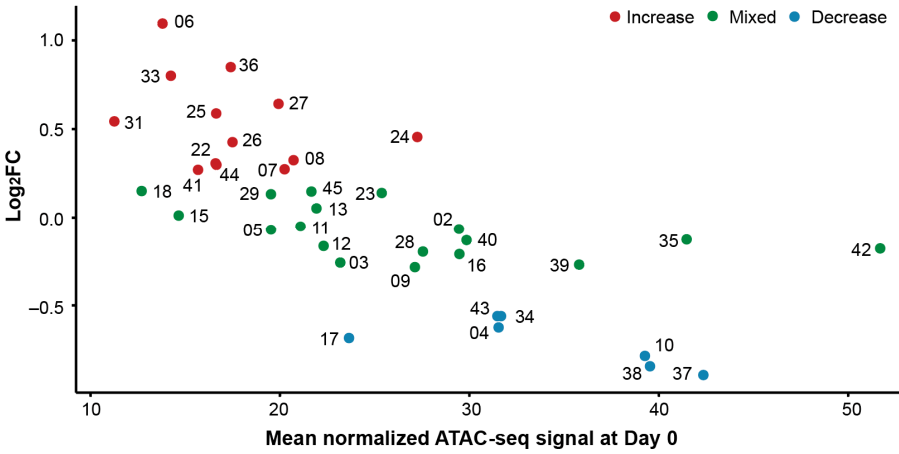


Figure 4. Relationship between basal chromatin accessibility and the acute ATAC-seq response to vitamin D_3. The scatter plot compares the participant-level mean ATAC-seq signal at baseline (Day 0) with the $\log_2$FC in mean accessibility 24 h after vitamin D_3 supplementation (Day 1 relative to Day 0). Each point represents one participant and is labeled with the participant number. Colors indicate classification as an accessibility-increase (red), mixed (green) or accessibility-decrease (blue) responder. Low basal accessibility was predominantly associated with a positive $\log_2$FC, whereas high basal accessibility was predominantly associated with a negative $\log_2$FC. Baseline signal contributes to both axes through the FC calculation; the plot therefore does not constitute an independent test of prediction.

CIBERSORTx estimates were examined to assess potential differences in PBMC composition between accessibility groups and sampling times (Figure S10). None of the 12 estimated cell fractions showed a statistically significant Day 0–Day 1 change within any

accessibility group after Benjamini–Hochberg correction across the 36 paired comparisons. The smallest adjusted *p*-value was observed for the estimated resting memory CD4 T-cell fraction in the accessibility-increase group ($p_{adj} = 0.150$). These results do not establish equivalent cellular composition or exclude smaller changes.

4. Discussion

This study identified substantial interindividual variation in normalized PBMC ATAC-seq signals 24 h after a body-weight-adjusted vitamin D_3 bolus. Exploratory accessibility groups differed in their observed signal trajectories and in the numbers of FDR-significant transcriptional responses. Baseline accessibility was also associated with subsequent change, although this relationship does not establish independent predictive value.

The accessibility-increase, mixed and accessibility-decrease categories represent an operational stratification of continuous variation. Because they were defined using the same paired measurements subsequently characterized, their accessibility patterns should not be interpreted as independent evidence for discrete biological responder phenotypes.

Predominantly increased accessibility has been reported following direct treatment of cellular models with $1,25(OH)_2D_3$ [7,28], including gains at 97.5% of strongly responsive regions in colonic organoids [7]. Moreover, higher aggregate ATAC-seq signal was reported in immortalized human endometrial stromal cells, together with both increased and decreased accessibility at individual regions [29]. Most vitamin D-responsive genes were associated with chromatin regions already accessible in vehicle-treated cells, consistent with transcriptional regulation within a pre-existing permissive chromatin landscape [29]. These findings emphasize the importance of cellular context when interpreting vitamin D responses. Regional gains and losses within a cell model should be distinguished from the opposing participant-level responses observed here. Differences across experimental systems may reflect cell identity and composition, conversion of vitamin D_3 to its active metabolite in vivo, exposure conditions and sampling time. Furthermore, the present results describe relative changes in normalized ATAC-seq signal and should not be interpreted as direct quantitative measurements of absolute genome-wide chromatin opening or closing.

The inverse association between basal accessibility and the subsequent response was one of the most prominent observations. Participants with relatively low pre-bolus accessibility generally showed increased accessibility, whereas those with higher basal accessibility tended to show a decrease. However, because the response measure incorporates the baseline value, mathematical coupling and regression to the mean may contribute to this inverse association. Independent prospective validation will be required to determine whether basal accessibility predicts subsequent molecular responses beyond mathematical coupling, regression to the mean and variation in library quality.

The candidate-region sets showed limited overlap and differences in their strongest motif enrichments. These observations suggest possible regulatory heterogeneity, although thresholding, unequal statistical power and selection of groups from the same ATAC-seq data may also contribute. Motifs recognized by hematopoietic transcription factors such as ETS1, NFY and BCL11B occurred in more than one group, whereas ATF1 and KLF5 motifs were preferentially enriched in accessibility-increase responders, ELF4 and SP1 motifs in mixed responders, and JUN-FOS motifs in accessibility-decrease responders. Motif enrichment identifies potential binding sequences but cannot demonstrate transcription factor occupancy or activity. Evaluation in independently defined groups, together with measurements of transcription factor occupancy or activity, would help determine whether these patterns reflect distinct regulatory responses.

Genetic variation may contribute to both basal accessibility and vitamin D responsiveness. In human colonic organoids, genetic variation was associated with interindividual

differences in chromatin accessibility and transcriptional responses to $1,25(OH)_2D_3$ [7]. Whether similar mechanisms contribute to the variation observed here remains to be tested by integrating genotype and ATAC-seq data.

The chromatin-based stratification was also reflected in the transcriptomic response. Accessibility-increase responders showed 74 FDR-significant differentially expressed genes, compared with eight in mixed responders and none in accessibility-decrease responders. These DEG counts alone do not establish differences in transcriptional effect size between groups or an absence of regulation in accessibility-decrease responders. Unequal group sizes and differences in variability affect statistical power, so the counts should be interpreted alongside the corresponding effect estimates. The enriched pathways in accessibility-increase responders involved interleukin, chemokine and T-cell receptor signaling and immune-cell differentiation, consistent with the established immunomodulatory functions of vitamin D [30,31].

RNA-seq-based deconvolution provided an indirect assessment of PBMC composition. Although no within-group changes met the specified multiple-testing threshold, this does not establish equivalence of composition or exclude smaller changes, particularly in the smallest group. The estimates depend on the reference signatures and may be influenced by activation-dependent gene expression. Reference labels such as macrophages or activated mast cells should therefore not be treated as direct identification of those populations in the isolated PBMCs. Deconvolution cannot independently demonstrate that the observed accessibility patterns are cell-intrinsic. Direct immunophenotyping and analyses of purified populations or single cells would help distinguish changes in abundance from regulation within individual cell types.

At the selected RNA-seq-significant loci, increased accessibility was frequently accompanied by lower steady-state transcript abundance. Accessibility indicates that DNA is available for regulatory interactions but does not specify whether those interactions promote or repress transcription. Recruitment of repressing complexes, secondary transcriptional responses, and differing temporal dynamics of chromatin accessibility, transcription and RNA turnover could produce discordant measurements at a single time point. These are possible explanations rather than mechanisms demonstrated by the present data.

Interpretation is also constrained by the selection of differentially expressed genes within the accessibility-increase group and by proximity-based assignment of distal peaks. The observations therefore do not establish a general inverse relationship between chromatin accessibility and transcription. Only three proximal and ten distal associations overlapped VDR-binding sites mapped in THP-1 cells [24]. This reference overlap supports candidate links to VDR but does not establish direct regulation in the sampled PBMCs. Conversely, absence of overlap cannot exclude VDR binding in another immune-cell type or activation state.

The paired sampling design, body-weight-adjusted dosing and integration of chromatin and transcriptomic measurements from the same participants are strengths of this study.

4.1. Limitations of the Study

The analysis includes 38 participants divided into small and unequal groups and examines one acute post-bolus time point without a time-matched untreated control. Changes following supplementation therefore cannot be fully separated from temporal and other concurrent influences or extrapolated to sustained supplementation. The accessibility groups and several downstream comparisons were derived from the same paired data, and most candidate ATAC-seq regions did not pass multiple-testing correction. Differences in group size and variability also affect the numbers of detected transcriptional responses.

The inverse baseline-change association is vulnerable to mathematical coupling and regression to the mean. Parallel changes in TSS enrichment and FRiP leave a contribution of library signal-to-background variation unresolved. Normalized ATAC-seq signals without an external quantitative reference do not establish absolute genome-wide chromatin opening or closing. Bulk PBMC measurements combine variation in cellular composition with regulation within cells, while RNA-based deconvolution does not independently measure cell abundance. Proximity-based peak-to-gene assignments and VDR annotations transferred from THP-1 cells further limit mechanistic interpretation.

4.2. Future Directions

Controlled longitudinal studies should test the reproducibility and persistence of these patterns using repeated baseline measurements and additional post-supplementation time points. Comparing bolus and sustained dosing would help distinguish acute responses from longer-term adaptation. Purified-cell or single-cell measurements, combined with direct immunophenotyping, could separate compositional changes from regulation within defined populations. Paired metabolite measurements and functional assessment of vitamin D signaling would help evaluate systemic availability and local metabolism. Any proposed predictor based on basal accessibility should use baseline information alone and undergo independent prospective validation, including assessment of its added value beyond serum 25(OH)D_3 and clinical characteristics.

5. Conclusions

Paired PBMC profiles revealed heterogeneous 24-h changes in normalized chromatin accessibility following vitamin D_3 supplementation. The largest number of FDR-significant transcriptional responses was detected in the accessibility-increase group, although group-specific discovery counts do not establish differences in response magnitude. The association between basal accessibility and subsequent change remains descriptive. Controlled longitudinal and cell-type-resolved studies are needed to assess reproducibility and determine whether chromatin measurements provide information beyond serum vitamin D status and clinical characteristics.

Supplementary Materials: The following supporting information can be downloaded at: https://www.mdpi.com/article/10.3390/nu18223777/s1, Table S1. Sequencing datasets and sample-level quality metrics; Table S2. Consensus ATAC-seq peaks and chromatin accessibility signals in PBMCs before and after vitamin D_3 supplementation;Table S3. Responder-group-specific RNA-seq analysis and association of genes with ATAC-seq peaks; Figure S1. Interindividual variation in PBMC chromatin accessibility following vitamin D_3 supplementation; Figure S2. Characterization of the PBMC chromatin accessibility response groups following vitamin D_3 supplementation; Figure S3. Genome-wide distribution of ATAC-seq signal intensities in the three response groups before and after vitamin D_3 supplementation; Figure S4. Genome-wide characterization and transcription factor motif enrichment of response-group-specific chromatin regions; Figure S5. Exploratory analysis of nominal transcriptional responses in the three chromatin responder groups; Figure S6. Chromatin accessibility at *NAMPT*- and *DUSP1*-associated regions in the three response groups; Figure S7. Functional enrichment of differentially expressed genes identified in accessibility-increase responders; Figure S8. ChromHMM annotation of accessible chromatin regions in the three vitamin D_3 response groups; Figure S9. Chromatin accessibility and gene expression changes across the three responder groups at RNA-seq-significant loci; Figure S10. Estimated immune-cell fractions before and after vitamin D_3 supplementation in the three chromatin responder groups.

Author Contributions: M.R. carried out data processing and interpretation with the support of R.G.D. and M.J.C., E.G. performed the experiments. The manuscript was written by C.C. and further refined by M.R. All authors have read and agreed to the published version of the manuscript.

Funding: This publication is part of the WELCOME2 project that has received funding from the European Union's Horizon 2020 research and innovation program under grant agreement no. 952601. In addition, this work was supported by a grant from the Polish National Science Centre NCN (grant no. 2023/49/B/NZ9/00402) to C.C. The funders had no role in the study design, data collection, data analysis, interpretation of the results or preparation of the manuscript.

Institutional Review Board Statement: The study protocol was approved by the Ethics Committee of the Olsztyn Chamber of Physicians (approval no. 31/2023/VIII; date: 11 September 2023). All procedures were conducted in accordance with the Declaration of Helsinki.

Informed Consent Statement: All participants provided written informed consent before participation.

Data Availability Statement: The raw sequencing data (FASTQ files) of ATAC-seq and RNA-seq are available at the Gene Expression Omnibus (GEO, www.ncbi.nlm.nih.gov/geo/) under accession numbers GSE303320 and GSE278885 (Table S1). The code used for the analyses is available in the GitHub repository at https://github.com/Maciej-EGM/VitDPAS_Reaserch.

Acknowledgments: The authors gratefully acknowledge the Gene Core facility at the European Molecular Biology Laboratory (EMBL), Heidelberg, Germany, for providing high-throughput sequencing services and the Centre of Informatics Tricity Academic Supercomputer and Network of Gdańsk University of Technology (https://task.gda.pl/en) for providing access to its computing resources.

Conflicts of Interest: The authors declare that they have no competing interests.

Abbreviations

$1,25(OH)_2D_3$	1α,25-dihydroxyvitamin D_3
$25(OH)D_3$	25-hydroxyvitamin D_3
ATAC-seq	Assay for transposase-accessible chromatin using sequencing
ATF1	Activating transcription factor 1
BCL11B	BCL11 transcription factor B
CCR5	C-C motif chemokine receptor 5
CD28	CD28 molecule
CD83	CD83 molecule
CDKN1A	Cyclin-dependent kinase inhibitor 1A
ChIP-seq	Chromatin immunoprecipitation sequencing
ChromHMM	Chromatin-state discovery and characterization using a hidden Markov model
CXCR4	C-X-C motif chemokine receptor 4
DEG	Differentially expressed gene
DUSP1	Dual-specificity phosphatase 1
ELF4	E74-like ETS transcription factor 4
ETS1	ETS proto-oncogene 1, transcription factor
FC	Fold change
FDR	False discovery rate
FRiP	Fraction of reads in peaks
HOMER	Hypergeometric Optimization of Motif EnRichment
IL	Interleukin
IL7R	Interleukin 7 receptor
JUN-FOS	Heterodimeric transcription factor formed by JUN and FOS proteins
KEGG	Kyoto Encyclopedia of Genes and Genomes
KLF	KLF transcription factor
NAMPT	Nicotinamide phosphoribosyltransferase
NFY	Nuclear transcription factor Y
PBMC	Peripheral blood mononuclear cell
PBX3	PBX homeobox 3
PCA	Principal component analysis
PD-1	Programmed cell death protein 1
PER1	Period circadian regulator 1
RNA-seq	RNA sequencing
S1PR1	Sphingosine-1-phosphate receptor 1

SOCS3	Suppressor of cytokine signaling 3
SP1	Sp1 transcription factor
STAR	Spliced Transcripts Alignment to a Reference
TFEC	Transcription factor EC
T_H	T helper cell
TNFAIP3	TNF alpha-induced protein 3
TSC22D3	TSC22 domain family member 3
TSS	Transcription start site
VDR	Vitamin D receptor

References

1. Baeke, F.; Takiishi, T.; Korf, H.; Gysemans, C.; Mathieu, C. Vitamin D: Modulator of the immune system. *Curr. Opin. Pharmacol.* **2010**, *10*, 482–496. [CrossRef] [PubMed]
2. Martens, P.J.; Gysemans, C.; Verstuyf, A.; Mathieu, C. Vitamin D's effect on immune function. *Nutrients* **2020**, *12*, 1248. [CrossRef] [PubMed]
3. Bishop, E.; Ismailova, A.; Dimeloe, S.K.; Hewison, M.; White, J.H. Vitamin D and immune regulation: Antibacterial, antiviral, anti-inflammatory. *JBMR Plus* **2021**, *5*, e10405. [CrossRef] [PubMed]
4. Chun, R.F.; Liu, P.T.; Modlin, R.L.; Adams, J.S.; Hewison, M. Impact of vitamin D on immune function: Lessons learned from genome-wide analysis. *Front. Physiol.* **2014**, *5*, 151. [CrossRef] [PubMed]
5. Haussler, M.R.; Haussler, C.A.; Bartik, L.; Whitfield, G.K.; Hsieh, J.C.; Slater, S.; Jurutka, P.W. Vitamin D receptor: Molecular signaling and actions of nutritional ligands in disease prevention. *Nutr. Rev.* **2008**, *66*, S98–S112. [CrossRef] [PubMed]
6. Seuter, S.; Virtanen, J.K.; Nurmi, T.; Pihlajamaki, J.; Mursu, J.; Voutilainen, S.; Tuomainen, T.P.; Neme, A.; Carlberg, C. Molecular evaluation of vitamin D responsiveness of healthy young adults. *J. Steroid Biochem. Mol. Biol.* **2017**, *174*, 314–321. [CrossRef] [PubMed]
7. Witonsky, D.; Laxman, B.; Usman, H.; Bielski, M.C.; Lawrence, K.M.; Kupfer, S.S. Genomic profiling of active vitamin D colonic responses in African- and European-Americans identifies an ancestry-related regulatory variant of POLB. *PLoS Genet.* **2026**, *22*, e1011983. [CrossRef] [PubMed]
8. Bikle, D.D. Vitamin D metabolism, mechanism of action, and clinical applications. *Chem. Biol.* **2014**, *21*, 319–329. [CrossRef] [PubMed]
9. Liu, P.T.; Stenger, S.; Li, H.; Wenzel, L.; Tan, B.H.; Krutzik, S.R.; Ochoa, M.T.; Schauber, J.; Wu, K.; Meinken, C.; et al. Toll-like receptor triggering of a vitamin D-mediated human antimicrobial response. *Science* **2006**, *311*, 1770–1773. [CrossRef] [PubMed]
10. Adams, J.S.; Ren, S.; Liu, P.T.; Chun, R.F.; Lagishetty, V.; Gombart, A.F.; Borregaard, N.; Modlin, R.L.; Hewison, M. Vitamin D-directed rheostatic regulation of monocyte antibacterial responses. *J. Immunol.* **2009**, *182*, 4289–4295. [CrossRef] [PubMed]
11. Heikkinen, S.; Väisänen, S.; Pehkonen, P.; Seuter, S.; Benes, V.; Carlberg, C. Nuclear hormone 1α,25-dihydroxyvitamin D_3 elicits a genome-wide shift in the locations of VDR chromatin occupancy. *Nucleic Acids Res.* **2011**, *39*, 9181–9193. [CrossRef] [PubMed]
12. Seuter, S.; Neme, A.; Carlberg, C. Epigenomic PU.1-VDR crosstalk modulates vitamin D signaling. *Biochim. Biophys. Acta* **2017**, *1860*, 405–415. [CrossRef] [PubMed]
13. Ramagopalan, S.V.; Heger, A.; Berlanga, A.J.; Maugeri, N.J.; Lincoln, M.R.; Burrell, A.; Handunnetthi, L.; Handel, A.E.; Disanto, G.; Orton, S.M.; et al. A ChIP-seq defined genome-wide map of vitamin D receptor binding: Associations with disease and evolution. *Genome Res.* **2010**, *20*, 1352–1360. [CrossRef] [PubMed]
14. Bell, O.; Tiwari, V.K.; Thoma, N.H.; Schubeler, D. Determinants and dynamics of genome accessibility. *Nat. Rev. Genet.* **2011**, *12*, 554–564. [CrossRef] [PubMed]
15. Buenrostro, J.D.; Giresi, P.G.; Zaba, L.C.; Chang, H.Y.; Greenleaf, W.J. Transposition of native chromatin for fast and sensitive epigenomic profiling of open chromatin, DNA-binding proteins and nucleosome position. *Nat. Methods* **2013**, *10*, 1213–1218. [CrossRef] [PubMed]
16. Gospodarska, E.; Ghosh Dastidar, R.; Jaroslawska, J.; Rybinski, M.; Raczyk, M.; Tokarczyk-Malesa, K.; Romaszko, J.; Carlberg, C. Transcriptomic profiling of immune modulation induced by vitamin D_3 in the VitDPAS and VitDHiD cohort studies. *Sci. Rep.* **2025**, *15*, 17334. [CrossRef] [PubMed]
17. Carlberg, C.; Haq, A. The concept of the personal vitamin D response index. *J. Steroid Biochem. Mol. Biol.* **2018**, *175*, 12–17. [CrossRef] [PubMed]
18. Hanel, A.; Neme, A.; Malinen, M.; Hamalainen, E.; Malmberg, H.R.; Etheve, S.; Tuomainen, T.P.; Virtanen, J.K.; Bendik, I.; Carlberg, C. Common and personal target genes of the micronutrient vitamin D in primary immune cells from human peripheral blood. *Sci. Rep.* **2020**, *10*, 21051. [CrossRef] [PubMed]
19. Love, M.I.; Huber, W.; Anders, S. Moderated estimation of fold change and dispersion for RNA-seq data with DESeq2. *Genome Biol.* **2014**, *15*, 550. [CrossRef] [PubMed]

20. Heinz, S.; Benner, C.; Spann, N.; Bertolino, E.; Lin, Y.C.; Laslo, P.; Cheng, J.X.; Murre, C.; Singh, H.; Glass, C.K. Simple combinations of lineage-determining transcription factors prime cis-regulatory elements required for macrophage and B cell identities. *Mol. Cell* **2010**, *38*, 576–589. [CrossRef] [PubMed]
21. Ernst, J.; Kellis, M. ChromHMM: Automating chromatin-state discovery and characterization. *Nat. Methods* **2012**, *9*, 215–216. [CrossRef] [PubMed]
22. Roadmap Epigenomics Consortium; Kundaje, A.; Meuleman, W.; Ernst, J.; Bilenky, M.; Yen, A.; Heravi-Moussavi, A.; Kheradpour, P.; Zhang, Z.; Wang, J. Integrative analysis of 111 reference human epigenomes. *Nature* **2015**, *518*, 317–330. [CrossRef] [PubMed]
23. Newman, A.M.; Steen, C.B.; Liu, C.L.; Gentles, A.J.; Chaudhuri, A.A.; Scherer, F.; Khodadoust, M.S.; Esfahani, M.S.; Luca, B.A.; Steiner, D.; et al. Determining cell type abundance and expression from bulk tissues with digital cytometry. *Nat. Biotechnol.* **2019**, *37*, 773–782. [CrossRef] [PubMed]
24. Fau, P.A.; Neme, A.; Seuter, S.; Carlberg, C. Temporal stratification of promoter-proximal versus enhancer VDR binding directs vitamin D-responsive transcription. *Epigenet. Chromatin* **2026**, *19*, 26. [CrossRef] [PubMed]
25. Kanehisa, M.; Furumichi, M.; Sato, Y.; Matsuura, Y.; Ishiguro-Watanabe, M. KEGG: Biological systems database as a model of the real world. *Nucleic Acids Res.* **2025**, *53*, D672–D677. [CrossRef] [PubMed]
26. Agrawal, A.; Balci, H.; Hanspers, K.; Coort, S.L.; Martens, M.; Slenter, D.N.; Ehrhart, F.; Digles, D.; Waagmeester, A.; Wassink, I.; et al. WikiPathways 2024: Next generation pathway database. *Nucleic Acids Res.* **2024**, *52*, D679–D689. [CrossRef] [PubMed]
27. Milacic, M.; Beavers, D.; Conley, P.; Gong, C.; Gillespie, M.; Griss, J.; Haw, R.; Jassal, B.; Matthews, L.; May, B.; et al. The Reactome pathway knowledgebase 2024. *Nucleic Acids Res.* **2024**, *52*, D672–D678. [CrossRef] [PubMed]
28. Jankowski, M.; Hamalainen, E.; Taipale, M.; Heikkinen, S.; Carlberg, C. Vitamin D and lipopolysaccharide jointly induce a distinct epigenetic and transcriptional program in human monocytes. *Sci. Rep.* **2025**, *15*, 27480. [CrossRef] [PubMed]
29. Yi, M.; Bostan, H.; DeMayo, F.J. Increased chromatin accessibility following 1α,25-dihydroxyvitamin D_3 treatment in human endometrial stromal cells. *Toxicol. Appl. Pharmacol.* **2026**, *516*, 118036. [CrossRef] [PubMed]
30. Yeh, W.Z.; Lea, R.; Stankovich, J.; Sampangi, S.; Laverick, L.; Van der Walt, A.; Jokubaitis, V.; Gresle, M.; Butzkueven, H. Transcriptomics identifies blunted immunomodulatory effects of vitamin D in people with multiple sclerosis. *Sci. Rep.* **2024**, *14*, 1436. [CrossRef] [PubMed]
31. Hewison, M. Vitamin D and immune function: An overview. *Proc. Nutr. Soc.* **2012**, *71*, 50–61. [CrossRef] [PubMed]

Disclaimer/Publisher's Note: The statements, opinions and data contained in all publications are solely those of the individual author(s) and contributor(s) and not of MDPI and/or the editor(s). MDPI and/or the editor(s) disclaim responsibility for any injury to people or property resulting from any ideas, methods, instructions or products referred to in the content.